Corneal Collagen Ordering After In Vivo Rose Bengal and Riboflavin Cross-Linking

James A. Germann,[1] Eduardo Martínez-Enríquez,[1] M. Carmen Martínez-García,[2] Irene E. Kochevar,[3] and Susana Marcos[1]

[1]Instituto de Óptica Consejo Superior de Investigaciones Cientificas, Madrid, Spain
[2]Departamento de Biología Celular, Histología y Farmacología, GIR de Técnicas Ópticas para el Diagnóstico, Universidad de Valladolid, Valladolid, Spain
[3]Wellman Center for Photomedicine, Massachusetts General Hospital and Harvard Medical School, Boston, Massachusetts, United States

Correspondence: James A. Germann, Instituto de Óptica Consejo Superior de Investigaciones Cientificas, C/Serrano, 121, Madrid 28006, Spain; j.germann@io.cfmac.csic.es.

Received: July 31, 2019
Accepted: December 10, 2019
Published: March 18, 2020

Citation: Germann JA, Martínez-Enríquez E, Martínez-García MC, Kochevar IE, Marcos S. Corneal collagen ordering after in vivo Rose Bengal and riboflavin cross-linking. *Invest Ophthalmol Vis Sci.* 2020;61(3):28. https://doi.org/10.1167/iovs.61.3.28

Purpose. Photoactivated cornea collagen cross-linking (CXL) increases corneal stiffness by initiating formation of covalent bonds between stromal proteins. Because CXL depends on diffusion to distribute the photoinitiator, a gradient of CXL efficiency with depth is expected that may affect the degree of stromal collagen organization. We used second harmonic generation (SHG) microscopy to investigate the differences in stromal collagen organization in rabbit eyes after corneal CXL in vivo as a function of depth and time after surgery.

Methods. Rabbit corneas were treated in vivo with either riboflavin/UV radiation (UVX) or Rose Bengal/green light (RGX) and evaluated 1 and 2 months after CXL. Collagen fibers were imaged with a custom-built SHG scanning microscope through the central cornea (350 µm depth, 225 × 225 µm en face images). The order coefficient (OC), a metric for collagen organization, and total SHG signal were computed for each depth and compared between treatments.

Results. OC values of CXL-treated corneas were larger than untreated corneas by 27% and 20% after 1 month and 38% and 33% after 2 months for the RGX and UVX, respectively. RGX OC values were larger than UVX OC values by 3% and 5% at 1 and 2 months. The SHG signal was higher in CXL corneas than untreated corneas, both at 1 and 2 months after surgery, by 18% and 26% and 1% and 10% for RGX and UVX, respectively.

Conclusions. Increased OC corresponded with increased collagen fiber organization in CXL corneas. Changes in collagen organization parallel reported temporal changes in cornea stiffness after CXL and also, surprisingly, are detected deeper in the stroma than the regions stiffened by collagen cross-links.

Keywords: cross-linking, second harmonic generation, rabbit eye, image analysis

Collagen fibril organization is a key factor in determining the strength,[1,2] stiffness,[2,3] and transparency[4] of the cornea along with factors such as proteoglycans[5] and hydration. Interweaving of collagen lamellae determines the stiffness of the different stromal layers[1] and the resistance of the cornea to swelling.[6,7] Stress, on both the lamellae and fiber layer, and strain can be determined by atomic force microscopy[8] and sheer loading,[9] respectively. Thus, estimating the collagen ordering and interweaving across the different corneal layers provides important information for both understanding the basic biomechanics of the cornea and the changes induced by surgery or disease.

One treatment aimed at strengthening the cornea is cross-linking (CXL). In photoactivated CXL, a photosensitizer is instilled in the cornea, which is then irradiated with light. The subsequent photochemical reactions initiate the formation of covalent bonds between collagen molecules or between collagen and other macromolecules. An increase in the corneal elastic modulus (by factors ranging from 1.6 to 10.7) immediately after CXL ex vivo has been demonstrated using several techniques to assess mechanical properties, including uniaxial stretching of corneal strips,[10,11] atomic force microscopy,[12] corneal or eye inflation,[13,14] flap extensiometry,[15,16] corneal deformation imaging,[17–19] elastography,[20,21] and Brillouin microscopy,[22] in rabbit, bovine, porcine, canine, and human eyes. There are only a few reports of in vivo CXL treatment in animal models, and several reports of these show that corneal strengthening persists (and may even increase) months after treatment.[16,23–25] Although most of the prior work relies on macroscopic mechanical measurements, changes occur at the fiber level and can be visualized microscopically on the level of the lamellae. How the order of the collagen lamellae varies with depth in the cornea and how changes evolve over time gives insights on the extent to which CXL affects collagen fibers and their arrangement.

Second harmonic generation (SHG) is a type of multiphoton microscopy where two excitation photons interact

with a non-centrosymmetric molecular structure to produce one emission photon without a loss of energy. SHG has been used to image collagen fibers in tumors,[26] tendons,[27,28] ovaries,[28] skin,[28] heart tissue,[29] sclera,[30] and cornea.[31] Several techniques have been developed for analyzing the resulting SHG collagen images, such as Fourier transform–based analysis,[32] Radon analysis,[33] structure tensor,[25] and fiber angle analysis.[2] Recently, we developed an order coefficient (OC) analysis method to quantify the lamellar order of porcine corneas that were CXL ex vivo.[31] The OC analysis allowed for automatic image analysis without the need for user input or additional modifications to a standard laser scanning microscope.

The purpose of this study was to determine the long-term effect of different CXL procedures on corneal collagen, specifically the organization of collagen fibers through the depth of the stroma. OC analysis of SHG images was used to quantify the differences between two different CXL procedures (riboflavin-UV light [UVX] and Rose Bengal–Green Light [RGX]) applied in vivo and analyzed 1 and 2 months after CXL.

Methods

Animal Model and CXL Treatments

Eyes were obtained from female adult albino New Zealand rabbits weighing between 2.5 to 3.0 kg and housed in the animal facilities at the University of Valladolid. The treatment protocols were approved by the Animal Ethics Committee at the University of Valladolid and complied with the ARVO Statement for the Use of Animals in Ophthalmic and Vision Research. Twelve eyes from eight rabbits were studied after the following treatments: (1) de-epithelialization only involving manual removal in an 8-mm diameter circle demarcated by a trephine. Two eyes were measured 1 month after CXL and two eyes measured at 2 months; (2) riboflavin-UV CXL (UVX) following the Dresden protocol.[34] A solution of 0.125% riboflavin-5-phosphate in 20% Dextran T500 (Farmacia Magistral, Madrid, Spain) was instilled on a de-epithelialized cornea at a rate of 1 drop every 5 minutes for 30 minutes. After the initial 30 minutes, the cornea was irradiated with an IROC UVA lamp (370 nm, 3 mW/cm^2; Institute for Refractive and Ophthalmic Surgery, Zurich, Switzerland) for 30 minutes with continued instilling of riboflavin solution at one drop every 5 minutes. Two eyes measured 1 month after CXL and two eyes measured after 2 months; and (3) RGX following the protocol developed by Cherfan et al.[35] A de-epithelialized eye was stained with 0.1% Rose Bengal in phosphate-buffered saline solution for 2 minutes and irradiated with a 532 nm laser (MGL-FN-532; Changchun New Industries, Changchun, China) with an irradiance of 0.25 W/cm^2 for 200 seconds. The cornea was restained for 30 seconds with the Rose Bengal solution and irradiated for an additional 200 seconds. Corneas measured 1 month after CXL came from rabbits where one eye was treated with a CXL procedure, either UVX or RGX, and the contralateral eye kept as a control. Corneas measured 2 months after CXL came from rabbits that were bilaterally treated with both CXL procedures. Control corneas were also obtained from rabbits of the same age and weight for comparison with the 2-month corneas. These rabbits were part of a larger study that addressed changes in the corneal biomechanical properties measured using air puff corneal deformation imaging[23] after the two different CXL modalities, as well as wound healing and histology with the RGX treatment.[36] SGH measurements were performed within 24 hours post mortem.

SHG Microscopy: Device, Imaging Protocols, and Analysis

A custom-developed SHG microscope, described in an earlier publication[31], was used for imaging. In brief, a Ti-sapphire pulsed laser source (Coherent MaiTai, 800 nm central wavelength) was focused with a high numerical aperture objective and frequency doubled light (i.e., 400 nm) was collected with a second high numerical aperture objective in the forward direction and single-photon counted with a photomultiplier tube.

En face images of central cornea collagen were taken in four 112.5 µm × 112.5 µm (300 pixels × 300 pixels) quadrants, giving a total measurement area of 225 µm × 225 µm (600 pixels × 600 pixels). Images were taken every 2 µm along the optical axis through a 350 µm depth, giving 175 total images collected in each z-scan. Although the average thickness of the New Zealand rabbit cornea was reported to be 400 to 500 µm,[37,38] analysis was limited to 350 µm to compensate for small variations in sample depth and because CXL effects are generally limited to the anterior 300 µm of the stroma.[35,39] Full volume collection of a cornea was obtained in 20 minutes.

The OC[31] analysis was implemented to determine the ordering of the collagen fibers in the rabbit cornea and further refined for the purposes of the current study. In short, the OC is the standard deviation of analysis points selected from the Fourier transformed image of the collagen fibers, with highest energy points selected for analysis. A variation of OC analysis was used in this study with the following modifications: (1) the analysis points of the Fourier transformed image were weighted by frequency, (2) the number of analysis points was set as the linear resolution of the image, and (3) overlapping windows were used in the analysis to avoid boundary artifacts. Overlapping windows of equal angular width present an advantage over static windows, because it is possible for bulk collagen orientation to straddle the window boundaries in the static case. Analysis windows were set at an angular width of 7.5° with an angular shift of 1.5° between adjacent windows. OC values were normalized to have a range between 0 and 1, where 0 represents an even distribution of collagen angles across all windows and 1 represents all the collagen fibers highly linear, that is, without kinks or bends, and oriented in one direction. The four quadrants of every image in the 225 µm × 225 µm x 350 µm volume were analyzed separately, assigned an OC, and then averaged.

Finally, the overall SHG signal at each depth was quantified by summing together all the individual pixel intensities of all four quadrants at every depth step. Average SHG values were computed for both the entire depth of the cornea and for the individual stromal sections divided into anterior (0–125 µm), intermediate (125–250 µm), and posterior stroma (250–350 µm). These section demarcations closely match the depth dependency of keratocyte density by stromal section.[40]

Results

Qualitative Assessment of SHG Images

The corneas measured in this experiment still had a yellow and rose tint in the UVX and RGX samples, respectively, both

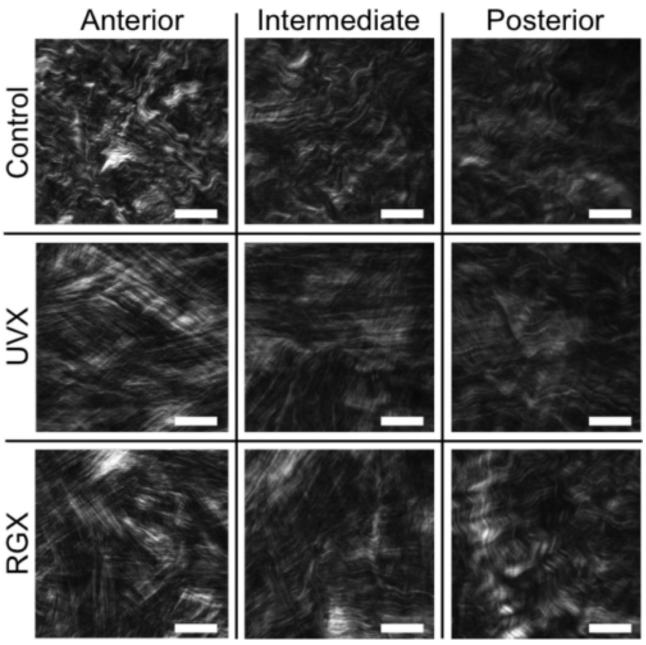

Figure 1. Representative SHG stromal collagen images from UVX, RGX, and control eyes taken from the anterior, intermediate and posterior sections of rabbit corneas 1-month after CXL. The anterior images were taken 60 µm below the anterior stromal surface, intermediate images were taken 180 µm below the anterior stromal surface, and posterior images were taken 300 µm below the anterior stromal surface. Contrast and brightness have been adjusted in the posterior control for easier viewing of the fibers. *White bars* in the corners of the images represent a distance of 25 µm.

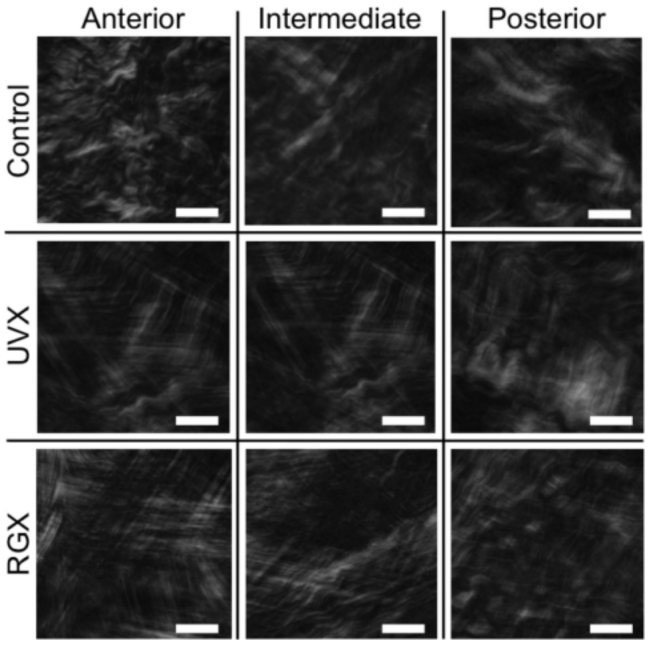

Figure 2. Representative SHG stromal collagen images from UVX, RGX, and control eyes taken from the anterior, intermediate, and posterior sections of rabbit corneas 2 months after CXL. The anterior images were taken 60 µm below the anterior stromal surface, intermediate images were taken 180 µm below the anterior stromal surface, and posterior images were taken 300 µm below the anterior stromal surface. *White bars* in the corners of the images represent a distance of 25 µm. Contrast and brightness were adjusted here to aid the reader for viewing the fibers.

1 and 2 months after CXL. Figures 1 and 2 show representative images of stromal collagen from the different treatments 1 and 2 months after treatment. Initial images were taken in all corneas near the anterior surface (0−20 µm), except for the 1-month UVX corneas, and were characterized by highly interwoven lamellae that are visualized as many short, disordered fibers. Differences between the CXL and control corneas become apparent in the range of approximately 20 to 125 µm, as fibers begin to collect into narrow lamellae (width 10–20 µm, examples shown in left column of Fig. 1). CXL lamellae found in these layers are still interwoven, but seemed to be more organized than the first 20 µm of anterior stroma. The control eyes also had narrow lamellae, but they seemed to be shorter in length. Images from the intermediate stroma (125−250 µm), especially from CXL samples, show a broadening of lamellar width and a continued elongation of the collagen fibers. The strong linearity of the CXL fibers began to give way to wavy fibers at approximately 170 µm below that anterior surface in both CXL cases and nearly all strands were completely wavy by 250 µm. These qualitative milestones of waviness hold for both the 1 and 2 months after CXL corneas and all treatment types.

Comparison of OC Values After Different CXL Treatments

One-Month After CXL. Figure 3 shows the OC values vs depth of all 1-month CXL samples and controls. The OC values of the RGX cornea are consistently higher than the control cornea, with an average RGX OC 27% larger ($P < 0.01$) than the average control OC across the entire stromal depth. The OC values of the UVX cornea, modeled here with a two-step function (high value 0.417, low value 0.307), are also greater than the control cornea in the anterior and intermediate layers, with the average UVX OC 20% larger ($P < 0.01$) than the average control OC. In rabbits receiving either RGX or UVX treatment (Fig. 3c) the average UVX OC was 3% larger than the RGX value across the entire stromal depth (averages significantly different $0.01 < P < 0.05$). In the 1-month UVX corneas, some lamellae suddenly stopped or were blunted in recorded images of the intermediate stroma, caused by lamellae slippage or fiber travel outside the imaging plane, examples of which are seen in Figure 4.

Two Months After CXL. Six eyes were analyzed 2 months after CXL. As in the 1-month corneas, the average OC of the controls was consistently lower than in CXL corneas by an average of 35.6% across the entire stroma ($P < 0.01$; RGX 38.0% larger, $P < 0.01$; UVX 33.1% larger, $P < 0.01$). Taken together, the average RGX OC of the two Gaussian curves was higher than the average UVX OC values by an average of 5.0% ($P < 0.01$). Taken separately, the average OC was not significantly different ($P > 0.05$) in the first UVX/RGX pair (Fig. 5a), but was significantly 13% higher ($P < 0.01$) for the RGX cornea in the second UVX/RGX pair (Fig. 5b). Peaks of the CXL fits are located close to 125 µm below the anterior surface, with the average Gaussian peak location at 126 µm and 120 µm for RGX and UVX corneas, respectively. From 1 month to 2 months after treatment, the OC as a function of depth remained linear in control corneas, and the differences in the absolute OCs are negligible. However, in CXL corneas, the average OC

Investigative Ophthalmology & Visual Science

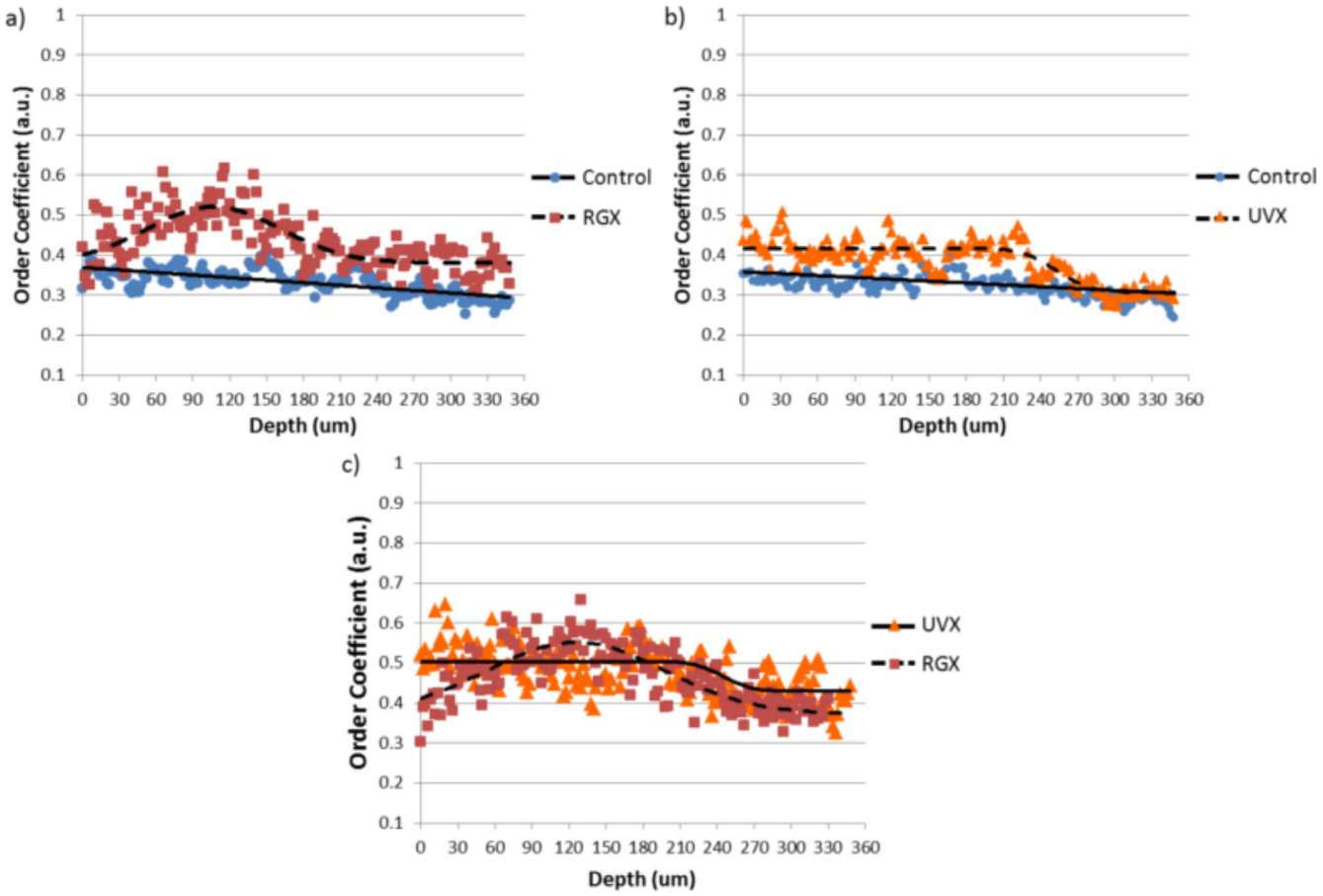

Figure 3. OC values of eyes from 1-month rabbits. (a) Contralateral pair of corneas with RGX treatment in one eye and other eye kept as control. (b) Contralateral pair of corneas with UVX treatment in one eye and other eye kept as control. (c) UVX and RGX treated corneas from different rabbits.

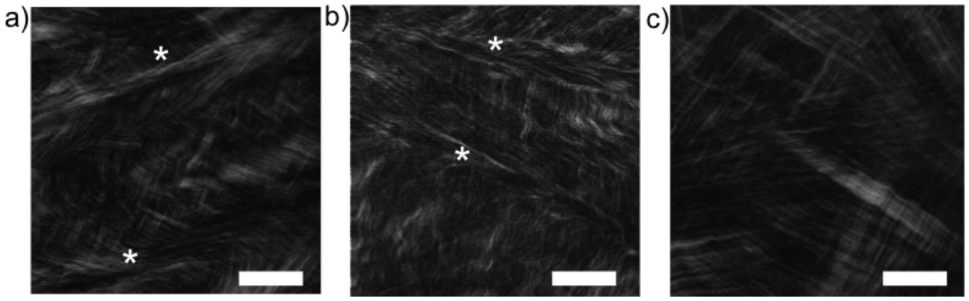

Figure 4. Collagen images from the deep anterior/intermediate UVX stroma. (a, b) From the 1-month samples. (c) From a 2-month sample. The depths of the images are (a) 114 µm, (b) 158 µm, and (c) 140 µm below the anterior stromal surface. The 1-month UVX corneas have some lamellae slippage in the intermediate stroma, highlighted with white asterisks, which introduced disorder into the lamellae images. *White bars* represent a distance of 25 µm.

increased across the entire cornea by 9.5% ($P < 0.01$) and by 7.7% ($P < 0.01$) in RGX and UVX treatments, respectively, from 1 month to 2 months after treatment.

SHG Image Intensity

Figure 6 shows the average SHG signal generated per image at 1 and 2 months after CXL. The SHG decreases significantly with depth (by 52.6% in control corneas [$P < 0.01$] and 24.5% in CXL corneas on average [$P < 0.01$], from anterior to posterior corneas), which is due to the scattering and attenuation of light inside the cornea. Although in control corneas there were no significant differences at 1 and 2 months after CXL in any corneal section ($P > 0.05$), SHG signal was significantly higher at 2 months than at 1 month after treatment in both CXL treatments and in all corneal sections (by 11.3%/2.7% [$P < 0.01$, $P < 0.01$] in the anterior, 8.1%/5.7% [$P < 0.01$, $P < 0.01$] in the

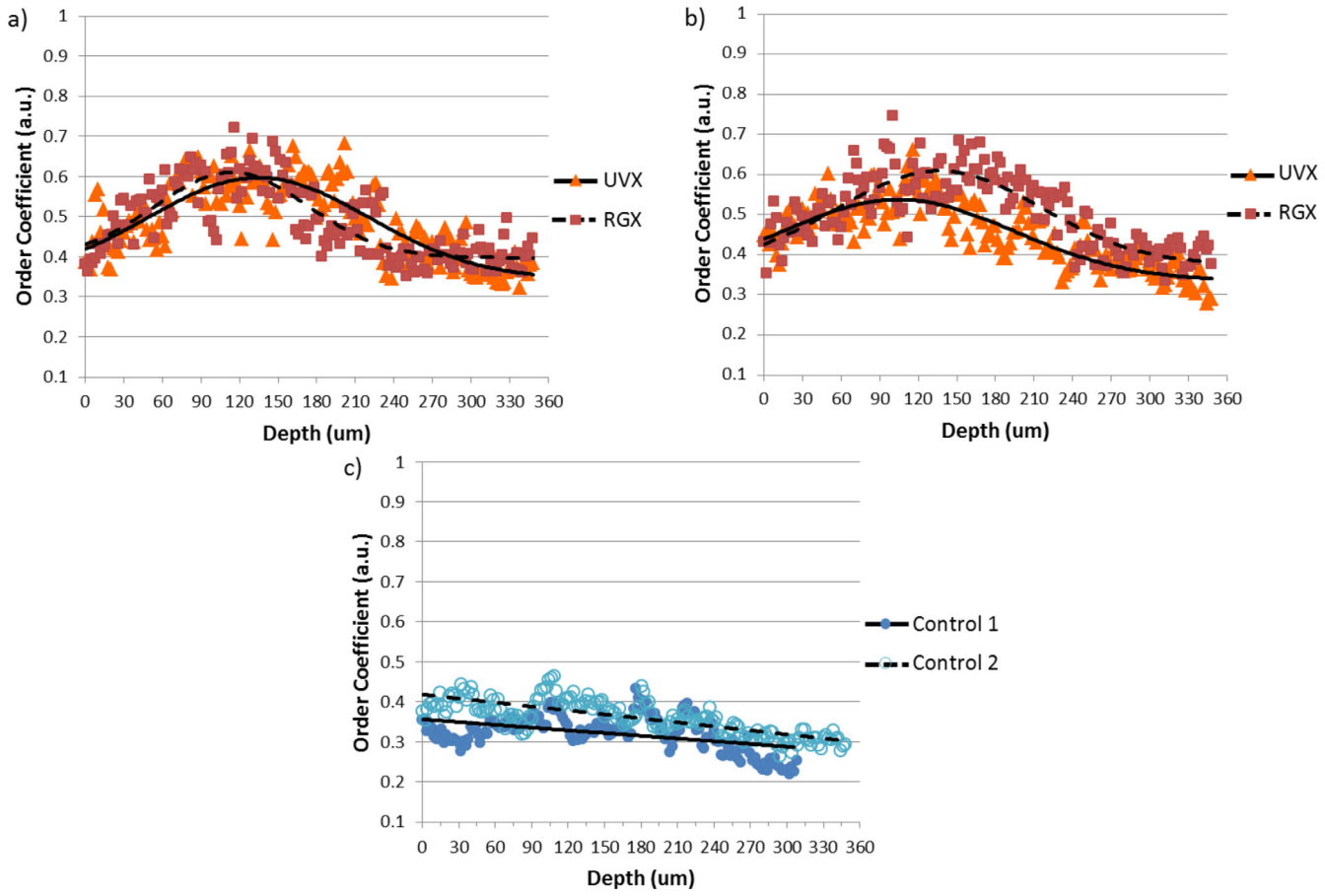

Figure 5. OC values of eyes from 2-month rabbits. (a, b) Contralateral pair of corneas with RGX treatment in one eye and UVX treatment in the other. (c) Two untreated corneas from different rabbits.

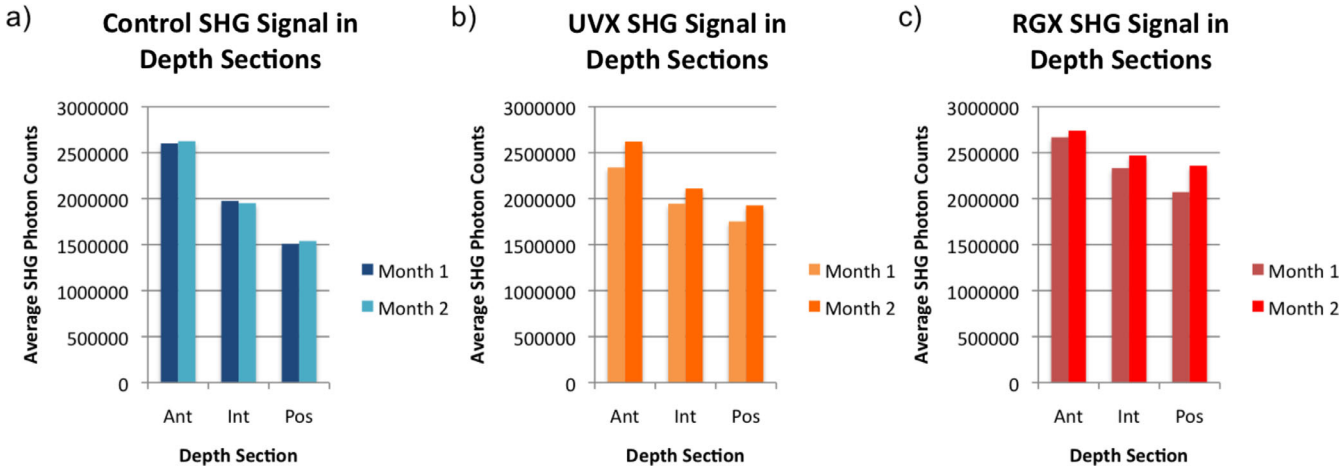

Figure 6. Average SHG by depth section, treatment, and month. (a) SHG signal from control corneas. (b) SHG signal from UVX corneas. (c) SHG signal from RGX corneas.

intermediate and 9.5%/13.0% [$P < 0.01$, $P < 0.01$] in the posterior for UVX/RGX, respectively). In general, the SHG signal for RGX corneas was higher than for UVX (18% at 1 month [$P < 0.01$], 12.5% at 2 months [$P < 0.01$], total cornea average), and higher than the control, except for the anterior section in the 1-month (15.5% at 1 month [$P < 0.01$], and 20.4% at 2 months [$P < 0.01$], total cornea average). The SHG signal for UVX was significantly higher than the control only in the posterior stroma (14.9% at 1 month [$P < 0.01$], and 22.3% at 2 months [$P < 0.01$]) and the intermediate stroma at 2 months (7.7% at 2 months [$P < 0.01$]). Otherwise, the average SHG signal of the UVX treated corneas was

not significantly different (intermediate 1 month, anterior 2 month, $P > 0.05$) or lower than in control corneas (10.5%, anterior at 1 month [$P < 0.01$]).

Discussion

We have shown that quantitative SHG imaging and analysis of collagen fibers can provide a quantitative marker of lamellae organization. In some aspects (in-depth variation in virgin; temporal variations after CXL), collagen organization correlates with collagen stiffening. Interestingly, increased values of the OC, compared with controls, extended deeper into the stroma than the regions previously shown to be stiffened, that is, beyond the anterior and mid-stroma[15,41] for UVX and the anterior stroma for RGX.[35] In RGX, the photosensitizer diffuses through the anterior 120 µm of the stroma,[35] and the riboflavin in UVX decreases from 0.1% to 0.082% after 300 µm in rabbit models,[42] which is the recorded CXL depth of UVX in some studies.[43] Sham controls in which riboflavin was applied without UV-A irradiation have demonstrated that riboflavin by itself does not significantly stiffen the stroma.[22] In addition, the increased collagen organization and linearity detected by the OC were still present 2 months after in vivo CXL. Our measurements also show that the average SHG signal in the CXL corneas generally increased from the 1 month to 2 month mark.

The shape of the OC curve as a function of depth varied between controls and CXL treatments. Control corneas showed modestly decreasing OC values as a function of depth, whereas after CXL two forms were observed, namely, a Gaussian curve for UVX and RGX at 2 months and for RGX at 1 month and a step function for UVX at 1 month, as shown in Figures 3 and 5. In corneas still attached to the ocular globe with IOP, the posterior stroma will be more ordered than the anterior stroma in the sense that the direction of the collagen fibers will be more uniform in the posterior stroma.[44] However, the measurements were done with the cornea removed from the ocular globe, which introduces kinks into the lamellae.[45] The kinks introduce greater variation in fiber direction and decrease the value of the OC. Based on previous reports of the depth distribution of stiffening,[22] the most superficial region of the cornea (0–50 µm) would be expected to experience the highest stiffening and OC value. However, for UVX at 2 months and for RGX at 1 and 2 months, the OC values were greater at a depth of around 100 to 120 µm (Figs. 3 and 5). This observation may reflect that in the 0- to 50-µm region the collagen lamellae are the most interweaved[46] and have a large variability in fiber direction in both treated and untreated corneas,[31] resulting in lower OC values. The anterior stromas of the CXL corneas do not see changes in fiber direction, most likely because the fibers are heavily interweaved and cannot move to become more aligned. As the depth increases past 50 µm, the individual fibers begin to coalesce into wider lamellae and lengthen (larger sections of the lamellae are captured in a single image plane), eventually broadening into lamellar sheets that, if perfectly straight, have a very high OC. However, CXL efficacy is also depth dependent because less photosensitizer reaches the posterior stroma and fewer photons reach the posterior stroma.[47] The peak of the Gaussian shapes is the point where the increase in OC from decreased interweaving and CXL-induced fiber linearity is maximized. Below the peak of OC values, fiber orientation becomes less uniform, although the OC never decreases to control levels. The OC versus depth curve for the 1-month UVX corneas (Fig. 3) was an exception to the Gaussian shape, which might be caused by stresses on the lamellae from CXL, SHG measurement, or changes in hydration (Fig. 4b).

In measuring the average SHG signal in the cornea, the amount of SHG recorded at each depth can be broken down into three factors: (1) total amount of SHG produced from the collagen fibers, (2) attenuation of the frequency doubled light in the stroma, and (3) attenuation of the excitation light, that is, 800-nm pulses. In the case of total SHG signal, the number of photons generated depends on the ordering and density of the collagen fibers, with a more ordered system producing more signal.[48] The ordering of collagen fibers is greater in CXL stromas owing to bonds being formed between the collagen fibrils or between the fibrils and the extracellular matrix.[49] This finding is clearly reflected in the average SHG measurements in the posterior and intermediate stroma, where the CXL stroma had a higher SHG average than the corresponding control depth. In the UVX corneas, the anterior stroma at both timepoints and intermediate stroma in the first month did not produce a significantly bigger average SHG than the control stroma and even less in the first month UVX. A likely reason for the lower signal in UVX is the non-zero one-photon absorption value of riboflavin at 400 nm,[50] which attenuates the total SHG signal. The calculated attenuation immediately after riboflavin installation, based on an average concentration of 3.79 mM and average path length of 175 µm, is approximately 44%. However, the true riboflavin concentration in the UVX stromas at 1 and 2 months after treatment is most likely lower than in the initial installation owing to transportation out of the cornea or by break down in the stroma. Rose Bengal does not have a substantial absorption at 400 nm.[51] Finally, attenuation of the excitation beam by collagen scattering may also affect the amplitude of the recorded SHG signal, with the photon penetration into the stroma following a ballistic model.[52] The transmission of 800 nm light through an undyed cornea with a thickness of 0.5 mm is 70% to 75%,[53] although the transmission through CXL stroma may be lower because the diameter of the fibers increases after CXL.[54] The one-photon absorbance of Rose Bengal and riboflavin at 800 nm is negligible, whereas the two-photon excitation of the dyes does not likely attenuate the excitation photons strongly. The zones of higher SHG signal match the OC analysis findings that greater organization is found in the posterior stroma of CXL corneas than in controls.

Our study shows an increase in the OC parameter with time after CXL. Interestingly, corneal biomechanical measurements of rabbit eyes after in vivo CXL have shown an increase in stiffness by a factor of 4.29 and 3.15, from 1 to 2 months after UVX and RGX, respectively.[23,24] Our results agree with these trends as shown by the increase in the linearity of the collagen fibers between 1 and 2 months for UVX corneas and the maintenance of increased linearity for RGX corneas during this period. These time-dependent effects in stromal remodeling may be attributable to CXL-activated stromal cells that produce cytokines and other mediators as well as creating new collagen fibers.[55] During this period, the stroma is repopulated by keratocytes, replacing those lost owing to photosensitization,[36,38] that may contribute to the matrix reorganization.

Our results indicate that CXL affects stroma structure at a depth deeper than the region in which stromal proteins are cross-linked. Stromal stiffening after CXL has been localized to the regions of high photosensitizer concentration

and light intensity by Brillouin microscopy,[22,35] phase decorrelation optical coherence tomography,[56] and stress–strain measurements of anterior/posterior CXL separated by a microkeratome.[15] For UVX, this region extends to the mid stroma in rabbit eyes and includes only the anterior stroma for RGX. A possible explanation for the collagen fiber changes in stromal regions in which cross-links are not formed rests on a biological response to effects of photosensitization in the cross-linked region. Cells damaged by photosensitization may secrete mediators that activate cells throughout the stroma, a response called the bystander effect.[57] This effect provides a mechanism for a localized damage site to affect distant sites in a tissue. Alternatively, the effect could arise purely from structural grounds, with the anterior collagen reorganization affecting the posterior structure, particularly in excised corneas.

The study design involved a relatively small sample to minimize the number of animals in the study. However, the measurements are robust, because each individual eye was measured at 175 different depths and each depth produced four separate analysis quadrants. Each individual image contains hundreds of collagen fibers that provide information on lamellae orientation and organization. Contralateral eyes were used to provide a more direct comparison between CXL treated and untreated eyes, as well as between different CXL treatments. The data collected are, therefore, sufficient to give an accurate description of the effects of CXL.

In summary, our results show that the impact of CXL in the cornea seems to affect a greater volume of the stroma than the volume where new bonds form, as seen from both OC analysis and the measurement of SHG at different depths. Organization of the collagen fibers at the microscopic level and the uniformity of orientation are correlated to the efficacy of CXL and increase of corneal stiffness. The findings of this study are in line with previous studies on CXL, with CXL affecting more greatly the anterior than the posterior stroma and the effects of CXL maintained or increased in the months after the treatment.

Acknowledgments

Supported by the European Research Council Advanced Grant ERC-2011-AdG Ref. 294099, Spanish Government Grants FIS2014-56643 and FIS2017-84753-R, H2020 Research and Innovation Action H2020-ICT-2017 Ref. 779960.

Disclosure: **J.A. Germann**, None; **E. Martínez-Enríquez**, None; **M.C. Martínez-García**, None; **I.E. Kochevar**, None; **S. Marcos**, None

References

1. Petsche SJ, Chernyak D, Martiz J, Levenston ME, Pinsky PM. Depth-dependent transverse shear properties of the human corneal stroma. *Invest Ophthalmol Vis Sci*. 2012;53:873–880.
2. Winkler M, Shoa G, Xie Y, et al. Three-dimensional distribution of transverse collagen fibers in the anterior human corneal stroma. *Invest Ophthalmol Vis Sci*. 2013;54:7293–7301.
3. Winkler M, Chai D, Kriling S, et al. Nonlinear optical macroscopic assessment of 3-D corneal collagen organization and axial biomechanics. *Invest Ophthalmol Vis Sci*. 2011;52:8818–8827.
4. Meek KM, Knupp C. Corneal structure and transparency. *Prog Retin Eye Res*. 2015;49:1–16.
5. Chen S, Mienaltowski MJ, Birk DE. Regulation of corneal stroma extracellular matrix assembly. *Exp Eye Res*. 2015;133:69–80.
6. Muller LJ, Pels E, Vrensen GF. The specific architecture of the anterior stroma accounts for maintenance of corneal curvature. *Br J Ophthalmol*. 2001;85:437–443.
7. DelMonte DW, Kim T. Anatomy and physiology of the cornea. *J Cataract Refract Surg*. 2011;37:588–598.
8. Labate C, Lombardo M, De Santo MP, Dias J, Ziebarth NM, Lombardo G. Multiscale Investigation of the depth-dependent mechanical anisotropy of the human corneal stroma. *Invest Ophthalmol Vis Sci*. 2015;56:4053–4060.
9. Sloan SR, Jr., Khalifa YM, Buckley MR. The location- and depth-dependent mechanical response of the human cornea under shear loading. *Invest Ophthalmol Vis Sci*. 2014;55:7919–7924.
10. Lanchares E, del Buey MA, Cristobal JA, Lavilla L, Calvo B. Biomechanical property analysis after corneal collagen cross-linking in relation to ultraviolet A irradiation time. *Graefes Arch Clin Exp Ophthalmol*. 2011;249:1223–1227.
11. Wollensak G, Spoerl E, Seiler T. Stress-strain measurements of human and porcine corneas after riboflavin-ultraviolet-A-induced cross-linking. *J Cataract Refract Surg*. 2003;29:1780–1785.
12. Dias J, Diakonis VF, Kankariya VP, Yoo SH, Ziebarth NM. Anterior and posterior corneal stroma elasticity after corneal collagen crosslinking treatment. *Exp Eye Res*. 2013;116:58–62.
13. Kling S, Remon L, Perez-Escudero A, Merayo-Lloves J, Marcos S. Corneal biomechanical changes after collagen cross-linking from porcine eye inflation experiments. *Invest Ophthalmol Vis Sci*. 2010;51:3961–3968.
14. Palko JR, Tang J, Cruz Perez B, Pan X, Liu J. Spatially heterogeneous corneal mechanical responses before and after riboflavin–ultraviolet-A crosslinking. *J Cataract Refract Surg*. 2014;40:1021–1031.
15. Kohlhaas M, Spoerl E, Schilde T, Unger G, Wittig C, Pillunat LE. Biomechanical evidence of the distribution of cross-links in corneas treated with riboflavin and ultraviolet A light. *J Cataract Refract Surg*. 2006;32:279–283.
16. Kling S, Ginis H, Marcos S. Corneal biomechanical properties from two-dimensional corneal flap extensiometry: application to UV-riboflavin cross-linking. *Invest Ophthalmol Vis Sci*. 2012;53:5010–5015.
17. Spoerl E, Terai N, Scholz F, Raiskup F, Pillunat LE. Detection of biomechanical changes after corneal cross-linking using ocular response analyzer software. *J Refract Surg*. 2011;27:452–457.
18. Bekesi N, Kochevar IE, Marcos S. Corneal biomechanical response following collagen cross-linking with rose Bengal-green light and riboflavin-UVA. *Invest Ophthalmol Vis Sci*. 2016;57:992–1001.
19. Dorronsoro C, Pascual D, Perez-Merino P, Kling S, Marcos S. Dynamic OCT measurement of corneal deformation by an air puff in normal and cross-linked corneas. *Biomed Opt Express*. 2012;3:473–487.
20. Twa MD, Li J, Vantipalli S, et al. Spatial characterization of corneal biomechanical properties with optical coherence elastography after UV cross-linking. *Biomed Opt Express*. 2014;5:1419–1427.
21. Touboul D, Gennisson JL, Nguyen TM, et al. Supersonic shear wave elastography for the in vivo evaluation of transepithelial corneal collagen cross-linking. *Invest Ophthalmol Vis Sci*. 2014;55:1976–1984.
22. Scarcelli G, Kling S, Quijano E, Pineda R, Marcos S, Yun SH. Brillouin microscopy of collagen crosslinking: noncontact depth-dependent analysis of corneal elastic modulus. *Invest Ophthalmol Vis Sci*. 2013;54:1418–1425.

Investigative Ophthalmology & Visual Science

23. Bekesi N, Gallego-Munoz P, Ibares-Frias L, et al. Biomechanical changes after in vivo collagen cross-linking with rose Bengal-green light and riboflavin-UVA. *Invest Ophthalmol Vis Sci*. 2017;58:1612–1620.
24. Zhu H, Alt C, Webb RH, Melki S, Kochevar IE. Corneal crosslinking with rose Bengal and green light: efficacy and safety evaluation. *Cornea*. 2016;35:1234–1241.
25. Bueno J, Avila F, Martinez- Garcia C. Quantitative analysis of the corneal collagen distribution after in vivo cross-linking with second harmonic microscopy. *Biomed Res Int*. 2019;2019:3860498.
26. Brown E, McKee T, diTomaso E, et al. Dynamic imaging of collagen and its modulation in tumors in vivo using second-harmonic generation. *Nat Med*. 2003;9:796–800.
27. Williams RM, Zipfel WR, Webb WW. Interpreting second-harmonic generation images of collagen I fibrils. *Biophys J*. 2005;88:1377–1386.
28. Cox G, Kable E, Jones A, Fraser I, Manconi F, Gorrell MD. 3-dimensional imaging of collagen using second harmonic generation. *J Struct Biol*. 2003;141:53–62.
29. Tiaho F, Recher G, Rouede D. Estimation of helical angles of myosin and collagen by second harmonic generation imaging microscopy. *Opt Express*. 2007;15:12286–12295.
30. Han M, Giese G, Bille J. Second harmonic generation imaging of collagen fibrils in cornea and sclera. *Opt Express*. 2005;13:5791–5797.
31. Germann JA, Martinez-Enriquez E, Marcos S. Quantization of collagen organization in the stroma with a new order coefficient. *Biomed Opt Express*. 2018;9:173–189.
32. Bueno JM, Palacios R, Chessey MK, Ginis H. Analysis of spatial lamellar distribution from adaptive-optics second harmonic generation corneal images. *Biomed Opt Express*. 2013;4:1006–1013.
33. Mega Y, Robitaille M, Zareian R, McLean J, Ruberti J, DiMarzio C. Quantification of lamellar orientation in corneal collagen using second harmonic generation images. *Opt Lett*. 2012;37:3312–3314.
34. Wollensak G, Spoerl E, Seiler T. Riboflavin/ultraviolet-a–induced collagen crosslinking for the treatment of keratoconus. *Am J Ophthalmol*. 2003;135:620–627.
35. Cherfan D, Verter EE, Melki S, et al. Collagen cross-linking using rose Bengal and green light to increase corneal stiffness. *Invest Ophthalmol Vis Sci*. 2013;54:3426–3433.
36. Gallego-Muñoz P, Ibares-Frías L, Lorenzo E, et al. Corneal wound repair after rose Bengal and green light crosslinking: clinical and histologic study. *Invest Ophthalmol Vis Sci*. 2017;58:3471–3480.
37. Chan T, Payor S, Holden BA. Corneal thickness profiles in rabbits using an ultrasonic pachometer. *Invest Ophthalmol Vis Sci*. 1983;24:1408–1410.
38. Lorenzo-Martín E, Gallego-Muñoz P, Ibares-Frías L, et al. Rose Bengal and green light versus riboflavin–UVA 1: corneal wound repair response. *Invest Ophthalmol Vis Sci*. 2018;59:4821–4830.
39. Brittingham S, Tappeiner C, Frueh BE. Corneal cross-linking in keratoconus using the standard and rapid treatment protocol: differences in demarcation line and 12-month outcomes standard versus rapid cross-linking treatment. *Invest Ophthalmol Vis Sci*. 2014;55:8371–8376.
40. Twa MD, Giese MJ. Assessment of corneal thickness and keratocyte density in a rabbit model of laser in situ keratomileusis using scanning laser confocal microscopy. *Am J Ophthalmol*. 2011;152:941–953 e941.
41. Webb JN, Langille E, Hafezi F, Randleman JB, Scarcelli G. Biomechanical impact of localized corneal cross-linking beyond the irradiated treatment area. *J Refract Surg*. 2019;35:253–260.
42. Gore DM, O'Brart DP, French P, Dunsby C, Allan BD. A comparison of different corneal iontophoresis protocols for promoting transepithelial riboflavin penetration. *Invest Ophthalmol Vis Sci*. 2015;56:7908–7914.
43. Seiler T, Hafezi F. Corneal cross-linking-induced stromal demarcation line. *Cornea*. 2006;25:1057–1059.
44. Morishige N, Petroll WM, Nishida T, Kenney MC, Jester JV. Noninvasive corneal stromal collagen imaging using two-photon-generated second-harmonic signals. *J Cataract Refract Surg*. 2006;32:1784–1791.
45. Krüger A, Hovakimyan M, Ramírez Ojeda DF, et al. Combined nonlinear and femtosecond confocal laser-scanning microscopy of rabbit corneas after photochemical cross-linking. *Invest Ophthalmol Vis Sci*. 2011;52:4247–4255.
46. Bueno JM, Gualda EJ, Artal P. Analysis of corneal stroma organization with wavefront optimized nonlinear microscopy. *Cornea*. 2011;30:692–701.
47. Spoerl E, Mrochen M, Sliney D, Trokel S, Seiler T. Safety of UVA-riboflavin cross-linking of the cornea. *Cornea*. 2007;26:385–389.
48. Couture C-A, Bancelin S, Van der Kolk J, et al. The impact of collagen fibril polarity on second harmonic generation microscopy. *Biophys J*. 2015;109:2501–2510.
49. Hayes S, Kamma-Lorger CS, Boote C, et al. The effect of riboflavin/UVA collagen cross-linking therapy on the structure and hydrodynamic behaviour of the ungulate and rabbit corneal stroma. *PLoS One*. 2013;8:e52860.
50. de Jesus MB, Fraceto LF, Martini MF, Pickholz M, Ferreira CV, de Paula E. Non-inclusion complexes between riboflavin and cyclodextrins. *J Pharm Pharmacol*. 2012;64:832–842.
51. Ludvíková L, Friš P, Heger D, Šebej P, Wirz J, Klán P. Photochemistry of rose Bengal in water and acetonitrile: a comprehensive kinetic analysis. *Phys Chem Chem Phys*. 2016;18:16266–16273.
52. Helmchen F, Denk W. Deep tissue two-photon microscopy. *Nat Methods*. 2005;2:932–940.
53. Doutch JJ, Quantock AJ, Joyce NC, Meek KM. Ultraviolet light transmission through the human corneal stroma is reduced in the periphery. *Biophys J*. 2012;102:1258–1264.
54. Wollensak G, Wilsch M, Spoerl E, Seiler T. Collagen fiber diameter in the rabbit cornea after collagen crosslinking by riboflavin/UVA. *Cornea*. 2004;23:503–507.
55. Song X, Stachon T, Wang J, Langenbucher A, Seitz B, Szentmary N. Viability, apoptosis, proliferation, activation, and cytokine secretion of human keratoconus keratocytes after cross-linking. *Biomed Res Int*. 2015;2015:254237.
56. Blackburn BJ, Gu S, Ford MR, et al. Noninvasive assessment of corneal crosslinking with phase-decorrelation optical coherence tomography. *Invest Ophthalmol Vis Sci*. 2019;60:41–51.
57. Mukherjee S, Chakraborty A. Radiation-induced bystander phenomenon: insight and implications in radiotherapy. *Int J Radiat Biol*. 2019;95:243–263.

Investigative Ophthalmology & Visual Science